Surface Wrinkling Patterns on a Core-Shell Soft Sphere

Bo Li,[1] Fei Jia,[1] Yan-Ping Cao,[1] Xi-Qiao Feng,[1,*] and Huajian Gao[2]

[1]*Center for Nano and Micro Mechanics & Institute of Biomechanics and Medical Engineering, Department of Engineering Mechanics, Tsinghua University, Beijing 100084, China*

[2]*School of Engineering, Brown University, Providence, Rhode Island 02912, USA*

(Received 9 February 2011; published 7 June 2011)

The three-dimensional patterns of surface wrinkling on a core-shell soft sphere are investigated through buckling and postbuckling analyses under differential tissue growth or shrinkage. With increasing deformation, the sphere first exhibits a buckyball-like wrinkling pattern and then undergoes a wrinkle-to-fold transition into labyrinth folded patterns, in agreement with experimental observations. This transition involves dynamic movement, rotation, and coalescence of polygons formed during the initial buckling.

DOI: 10.1103/PhysRevLett.106.234301 PACS numbers: 46.32.+x, 81.40.Jj

Soft materials such as elastomers and polymeric gels are promising a wide range of applications from optical sensing or actuation to biomedical engineering [1]. While these materials can swell or shrink in response to external stimuli (e.g., pH, humidity, and temperature), soft biological tissues such as muscles and arteries undergo growth and atrophy under various physiological or pathological conditions. Mechanics of soft materials associated with swelling or shrinking has attracted considerable attention [2]. Much experimental effort has been directed toward the synthesis of core-shell structured hydrogels [3], with potential applications for drug delivery, enzyme supports, and biosensors. In such structures, the differential swelling or shrinking that originates from nonuniform physical and chemical properties or physiological changes can elicit stresses and trigger various morphological instabilities [4,5].

The phenomenon of surface wrinkling, as exemplified in nature by shriveled apples, dried raisins and dehydrated peas, is, on one hand, a nuisance to be avoided in many engineering applications and, on the other hand, a useful way of achieving unusual physical properties such as superhydrophobicity and self-cleaning. Recently, the buckling and postbuckling behaviors of a planar stiff film resting on a soft substrate subjected to in-plane compression [6–9] or lifted by a probe [10] have been studied both experimentally and theoretically. Because of topological constraints, the buckling patterns on curved surfaces can be quite different from those on planar surfaces [11], and three-dimensional (3D) surface buckling and postbuckling behaviors of a nonplanar layered structure are still elusive. In this Letter, we investigate the dynamic evolution of surface wrinkling patterns on a soft sphere with hard skin induced by tissue growth or shrinkage. The problem under consideration involves a spherical core-shell configuration which can model, for example, growing tumors, hydrogel core-shell particles, and many types of fruits.

We analyze the inhomogeneous deformation, buckling and postbuckling behaviors of a soft core-shell sphere within the framework of finite elasticity. The volumetric growth model originally established for biological tissues [12–14] is adopted to describe the inhomogeneous expansion or shrinkage. We use the spherical coordinate system $\mathbf{X} = (R, \Theta, \Phi)$ for the initial configuration and $\mathbf{x} = (r, \theta, \phi)$ for the current configuration, as shown in Fig. 1.

According to the volumetric growth theory [12], the deformation gradient $\mathbf{F} = \partial\mathbf{x}/\partial\mathbf{X}$ can be decomposed multiplicatively as $\mathbf{F} = \mathbf{A} \cdot \mathbf{G}$, where $\mathbf{G}$ denotes the growth tensor describing the addition (growth) or reduction (shrinkage) of materials and $\mathbf{A}$ is the elastic deformation tensor, which ensures the compatibility and continuity of deformation. For the sake of simplicity, here we assume that the materials swell or shrink isotropically. Without loss of generality, we further assume that shrinking takes place only in the core and can be characterized by an isotropic tensor $\mathbf{G} = g\mathbf{I}$, where g $(0 < g < 1)$ is a constant and $\mathbf{I}$ is the unit tensor. The relative magnitude of shrinking is measured by $\bar{g} = 1 - g$, hereafter referred to as the shrinking factor. In view of the spherical symmetry of the system, the elastic deformation tensor can be expressed as $\mathbf{A} = \mathrm{diag}(\alpha_1, \alpha_2, \alpha_3)$, where $\alpha_1 = g^{-1}\partial r/\partial R$ and $\alpha_2 = \alpha_3 = \alpha = g^{-1}r/R$. In the case of simultaneous swelling or shrinking of the shell and the core, both the method of

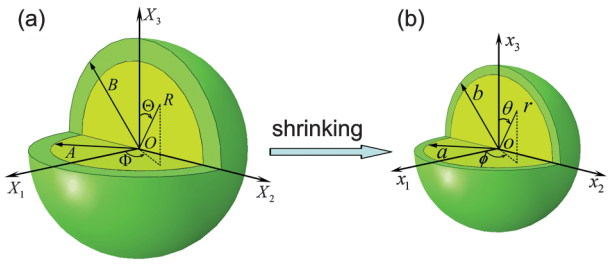

FIG. 1 (color). Shrinking of a soft sphere with a hard skin layer: (a) initial configuration and (b) current configuration.

analysis and the conclusions would be very similar to the case under study.

The incompressible neo-Hookean model with strain energy function $W = \frac{1}{2}\mu(\alpha_1^2 + \alpha_2^2 + \alpha_3^2 - 3)$ is used to characterize the nonlinear constitutive behavior of the material, where μ is the shear modulus. Elastic incompressibility requires $\det\mathbf{A} = 1$, which leads to $J = \det\mathbf{F} = \det\mathbf{G}$. The total potential energy of the system is

$$U = \int_\Omega J[W - p(\det\mathbf{A} - 1)]d\Omega, \tag{1}$$

where p is a Lagrangian multiplier and Ω the initial volume occupied by the sphere. Minimization of Eq. (1) yields the mechanical equilibrium for the system [15].

The incremental deformation theory accounting for growth or shrinkage effect [13,16] will be utilized to analyze the morphological stability of the core-shell sphere. The stability analysis proceeds by solving the incremental equilibrium equation $\mathrm{div}\dot{\mathbf{S}}_0 = \mathbf{0}$ in conjunction with the perfect bonding conditions at the core-shell interface, where $\dot{\mathbf{S}}_0$ is the incremental nominal stress.

The wrinkling mode of such a soft sphere can be well characterized by a spherical harmonic function $Y_l^m(\theta, \phi)$ of degree l and order m, which characterize the wrinkling modes in the longitudinal and latitudinal directions, respectively [17]. Combining this with the incremental equilibrium equation leads to an ordinary differential equation determining the critical condition of surface wrinkling [15].

Let $\bar{g}_{\mathrm{crit}}$ denote the critical shrinking factor at the occurrence of surface wrinkling. The corresponding surface pattern after buckling is described by its critical mode number, l_{crit}, which minimizes the total energy of the system among all possible modes. Figure 2 shows good agreement between the theoretical solutions [15] and our numerical results of finite element method (FEM). It is found that $\bar{g}_{\mathrm{crit}}$ increases with the shell thickness H [Fig. 2(a)]. Since the Föppl–von Kármán number $\gamma \sim (A/H)^2$, which characterizes the relative importance of stretch and bending rigidities [18], the critical shrinking factor $\bar{g}_{\mathrm{crit}}$ decreases as γ increases. In addition, a larger shrinking factor $\bar{g}_{\mathrm{crit}}$ is needed to destabilize spheres with a smaller ratio, μ_s/μ_c, between the shear moduli of the shell and the core [Fig. 2(b)]. It is shown that l_{crit} can be lowered either by increasing H/A or μ_s/μ_c.

Besides the surface buckling pattern, the characteristic of dynamic morphological evolution in the subsequent postbuckling deformation is also of great interest [19] but has received less attention previously. In order to investigate the spatial topographical evolution during postbuckling, we further perform 3D FEM simulations in a wide range of geometric and material parameters by using a pseudodynamic solution method [14]. As will be shown below, this method can well capture the complicated evolution process from initial isotropic deformation, buckling, to postbuckling with large deformation.

The displacement and elastic energy density distributions on the shell surface are depicted in Figs. 3(a)–3(h), respectively. Initially, the sphere shrinks isotropically and the energy distribution is uniform [Figs. 3(a) and 3(e)]. When the shrinkage reaches a critical value, the sphere suddenly bifurcates into a periodic dimple structure. Correspondingly, the energy distribution in the sphere evolves into a discrete but periodic profile. To further investigate the buckling mechanism, Fig. 4 plots the normalized total energy $\bar{U}$ of the system as a function of the shrinking factor $\bar{g}$. The energy variation from FEM simulation is in good agreement with the theoretical solution [Eq. (1)] before the occurrence of buckling (region I). When the shrinkage exceeds a critical value, $\bar{g}_{\mathrm{crit}}$, the spherical surface buckles and the system enters into region II as a consequence of energy minimization. With further shrinking, a pattern consisting of regular pentagons and hexagons characterizes the surface of the sphere, as shown in Figs. 3(b) and 5(a). Our numerical simulations confirm that this configuration is energetically favorable.

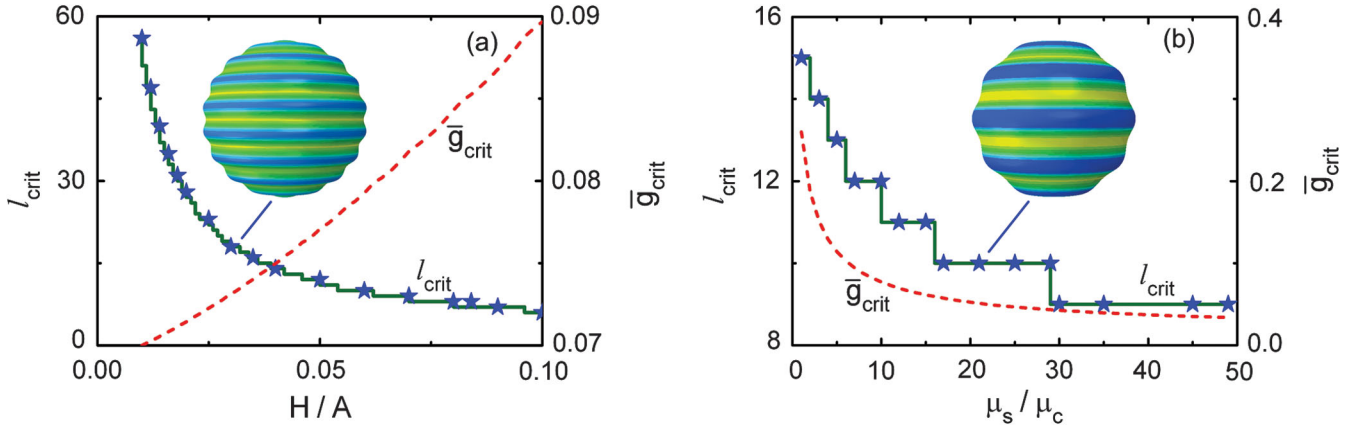

FIG. 2 (color). Dependence of the critical shrinking factor $\bar{g}_{\mathrm{crit}}$ (dashed line) and mode number l_{crit} (solid line and stars) on (a) the normalized initial shell thickness H/A and (b) the modulus ratio μ_s/μ_c. In (a), $\mu_s/\mu_c = 10$ and in (b) $H/A = 0.05$. The numerical results of FEM (stars) agree well with theoretical predictions (solid line).

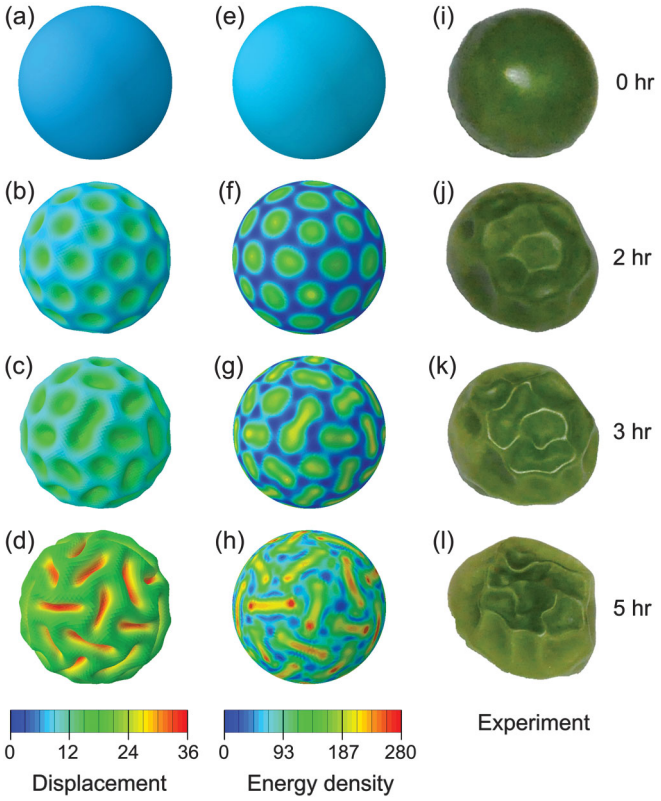

FIG. 3 (color). FEM simulations and experimental observations of surface wrinkling in a core-shell sphere. The left column shows the evolution of surface morphology with increasing shrinkage: (a) isotropic shrinking, (b) buckyball pattern, (c) deformed polygons, and (d) labyrinth topography. The middle column illustrates the evolution of energy density on the spherical surface: (e)–(h) are the energy density distributions corresponding to (a)–(d), respectively. In the calculation, we took $A = 100$, $B = 104$, and $\mu_s/\mu_c = 10$. The right column shows the surface pattern transition of a gradually dehydrated green pea in a dry environment. Time for (i)–(l) is 0, 2, 3, and 5 hours, respectively.

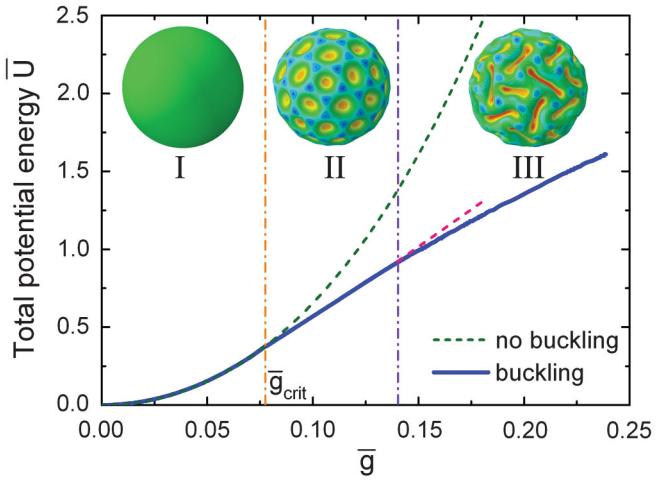

FIG. 4 (color). Variation of the normalized total potential energy $\bar{U} = U/(\mu_c A^3)$ with the shrinking factor $\bar{g}$. In region I, the sphere shrinks isotropically. Before buckling, the theoretically calculated total energy (green dashed line) fits well with numerical simulations (solid line). In region II, the system buckles into a buckyball configuration to lower energy. In region III, a second bifurcation takes place, corresponding to a wrinkling-to-fold transition. Red dashed line means no secondary bifurcation. Here, we took $A = 100$, $B = 104$, and $\mu_s/\mu_c = 10$.

Such a pattern is reminiscent of the structure of C_{60} [Fig. 5(b)] and hence referred to as the buckyball-like pattern.

As the shrinkage increases further, a second bifurcation may take place and the system enters into region III [Fig. 4]. The buckyball pattern from the first bifurcation breaks into foldlike structures: some polygons narrow into troughs, while others merge with their neighbors [Fig. 3(c)]. Correspondingly, the periodicity of energy distribution is also broken [Fig. 3(g)]. During the postbuckling process, the troughs deepen and the ridges sharpen, leading to a wrinkle-to-fold transition. In comparison with the buckyball pattern, the folding patterns can release more elastic strain energy in this stage, as shown in Fig. 4. This surface morphological evolution as $\bar{g}$ is increased involves the movement and rotation of ridges, just like the evolution of bonds during defect formation in fullerenes. Finally, the

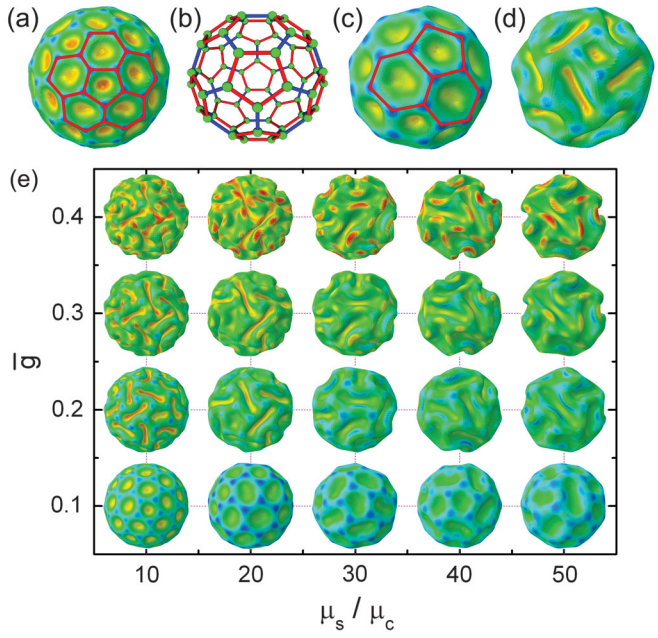

FIG. 5 (color). Buckyball and labyrinthine patterns of surface wrinkling. (a) Pentagons and hexagons incurred by the first bifurcation and (b) the structure of C_{60}. Postbuckling of a core-shell sphere: (c) buckyball pattern and (d) furrowed topography. (e) Evolutions of the surface morphologies of spheres with different values of μ_s/μ_c. In (a), $A = 100$, $B = 104$, and $\mu_s/\mu_c = 10$; in (c) and (d), $A = 100$, $B = 106$, and $\mu_s/\mu_c = 10$; in (e), $A = 100$ and $B = 104$.

spherical surface evolves toward a labyrinthine pattern [Fig. 3(d)], corresponding to the further localization of elastic strain energy [Fig. 3(h)]. Our FEM simulations also demonstrate that increasing either the shell thickness or the modulus ratio μ_s/μ_c will reduce the mode number (or enhance the wavelength) of the 3D surface patterns, as shown in Figs. 5(c)–5(e). For several representative values of μ_s/μ_c, Fig. 5(e) shows the surface morphological evolution of spheres with increasing $\bar{g}$ during postbuckling.

To corroborate our theoretical findings, we have experimentally observed the drying of green peas, which have a core-shell structure consisting of a spherical seed coated by a harder testa layer, just like the configuration shown in Fig. 1. In the initial state, the fresh peas have a high content of water and a smooth surface [Fig. 3(i)]. Then they are gradually dehydrated in a dry environment. Because of higher water content in the core, the seed has a larger shrinking factor than the coat, yielding a compressive stress in the shell layer. Figures 3(j)–3(l) show representative examples for comparison with our theoretical prediction. It is seen that differential shrinkage can cause multiple steps of symmetry breaking, giving rise to a 3D pattern on the curved surface. More specifically, the pea first shrinks isotropically, followed by buckyball-like buckling and then folding. These observations corroborate well with our theoretical predictions.

In summary, we have investigated surface buckling and morphological transition of a core-shell soft sphere by using a volumetric growth theory of finite deformation. The critical buckling condition and induced patterns are found to be sensitive to the shell thickness (represented by the Föppl–von Kármán number) and mechanical properties of the sphere. Both numerical simulations and experimental observations demonstrate that the sphere tends to buckle into a buckyball pattern at the initial bifurcation, followed by a wrinkle-to-fold transition that leads to the formation of a labyrinthine topography on the curved surface at subsequent bifurcations. Understanding the nonlinear buckling and morphological transition of soft spheres is not only beneficial for applications in medical engineering but also promises interesting fabrication routes to multifunctional surfaces.

Supports from NSFC (Grants No. 10972121, No. 10732050 and No. 10525210), Tsinghua University (2009THZ02122) and the 973 Program of MOST (2010CB631005) are acknowledged.

*fengxq@tsinghua.edu.cn

[1] A. Sidorenko *et al.*, Science **315**, 487 (2007); J. Kim, J. Yoon, and R. C. Hayward, Nature Mater. **9**, 159 (2010).
[2] W. Hong, X. Zhao, J. Zhou, and Z. Suo, J. Mech. Phys. Solids **56**, 1779 (2008).
[3] S. Nayak and L. A. Lyon, Angew. Chem., Int. Ed. **44**, 7686 (2005).
[4] E. Cerda and L. Mahadevan, Phys. Rev. Lett. **90**, 074302 (2003).
[5] N. Tsapis *et al.*, Phys. Rev. Lett. **94**, 018302 (2005).
[6] L. Pocivavsek *et al.*, Science **320**, 912 (2008).
[7] F. Brau *et al.*, Nature Phys. **7**, 56 (2011).
[8] J. Y. Sun, S. Xia, M. Y. Moon, K. H.Oh, and K. S. Kim, "Folding Wrinkles of a Thin Stiff Layer on a Soft Substrate." (unpublished).
[9] S. Cai, D. Breid, A. J. Crosby, Z. Suo, and J. W. Hutchinson, J. Mech. Phys. Solids **59**, 1094 (2011).
[10] D. P. Holmes and A. J. Crosby, Phys. Rev. Lett. **105**, 038303 (2010).
[11] P. D. Shipman and A. C. Newell, Phys. Rev. Lett. **92**, 168102 (2004); C. Li, X. Zhang, and Z. Cao, Science **309**, 909 (2005); G. Cao *et al.*, Phys. Rev. Lett. **100**, 036102 (2008).
[12] E. K. Rodriguez, A. Hoger, and A. McCulloch, J. Biomech. **27**, 455 (1994).
[13] A. Goriely and M. Ben Amar, Phys. Rev. Lett. **94**, 198103 (2005); J. Dervaux and M. Ben Amar, Phys. Rev. Lett. **101**, 068101 (2008).
[14] N. Stoop *et al.*, Phys. Rev. Lett. **105**, 068101 (2010).
[15] See supplemental material at http://link.aps.org/supplemental/10.1103/PhysRevLett.106.234301 for complete derivation.
[16] B. Li, Y. P. Cao, X. Q. Feng, and H. Gao, J. Mech. Phys. Solids **59**, 758 (2011).
[17] A. S. D. Wang and A. Ertepinar, Int. J. Non-Linear Mech. **7**, 539 (1972).
[18] J. Lidmar, L. Mirny, and D. R. Nelson, Phys. Rev. E **68**, 051910 (2003).
[19] H. Aharoni and E. Sharon, Nature Mater. **9**, 993 (2010).